Supplementary material

Enhancing High-Temperature Capacitive Energy Storage Performance of BOPP Films via Constructing a Dual-barrier Structure

Tianyuan Yin[2], Bize Gong[2], Hai Sun[2], Chao Yin[23], Yue Zhang[23], Changhai Zhang[23], Tiandong Zhang[123]*

1 School of Electrical and Electronic Engineering, Harbin University of Science and Technology, Harbin
150080, PR China
2 National Key Laboratory of High-performance Special Cable Technology, Harbin 150080, PR China
3 Key Laboratory of Engineering Dielectrics and Its Application, Ministry of Education, Harbin University
of Science and Technology, Harbin 150080, PR China

#Co-first authors: Tianyuan Yin, Bize Gong
*Corresponding author: Tiandong Zhang
E-mail: tdzhang@hrbust.edu.cn

Fitting of hopping conduction current density:

The current density generated by hopping conduction can be expressed as:

$$J = 2\mathrm{nq}\lambda\nu \exp(-\frac{W_a}{K_B T}) \sinh(\frac{\lambda \mathrm{q} E}{2K_B T})$$

Where q is the charge of the carriers, n is the carrier density, λ is the average hopping distance, ν is the attempt-to-escape frequency, W_a is the activation energy of hopping conductance, k_B is the Boltzmann constant, T is the absolute temperature and E is the applied electric field. That can be simplified as:

$$J = \alpha \sinh(\beta E)$$

$$\alpha = 2\mathrm{nq}\lambda\nu \exp(-\frac{W_a}{K_B T})$$

$$\beta = \frac{\lambda \mathrm{q}}{2K_B T}$$

Fitting of Schottky injection current density:

Schottky injection current density can be expressed by:

$$J = AT^2 \exp\left(\frac{-q(\phi_B - \sqrt{qE/4\pi\varepsilon_r\varepsilon_0})}{k_B T}\right)$$

Where A is the Richardson constant, T is the absolute temperature, q is the charge of the carrier, $q\phi B$ is the Schottky injection barrier, E is the applied electric field, ε_0 is the vacuum dielectric constant, ε_r is the relative dielectric constant, k_B is the Boltzmann constant. The above formula can be equivalently transformed into:

$$\ln(\frac{J}{T^2}) = \left(\frac{\sqrt{q^3/4\pi\varepsilon_r\varepsilon_0}}{k_B T}\right)\sqrt{E} + \ln(A) - \left(\frac{q\phi_B}{k_B T}\right)$$

For the Schottky injection emission, the relationship between $\ln(J/T^2)$ and $E^{1/2}$ is linear. The linear fitting results of $\ln(J/T^2)$ on $E^{1/2}$ can be used to determine whether the Schottky injection is the dominant conduction mechanism.

Weibull distribution of breakdown field strength：

The breakdown strength test for composite films is based on the statistical distribution following the Weibull distribution (Formula), with the sample size of 10 per test. E_i denotes the breakdown strength of the i^{th} sample, and E_b corresponds to the characteristic breakdown strength associated with a breakdown probability of 63.2%. β is the shape parameter used to assess the degree of data dispersion, reflecting the stability of the composite film's breakdown strength.

$$\mathrm{P(E)} = 1 - \exp[-\left(\frac{\mathrm{E_i}}{\mathrm{E_b}}\right)^{\beta}]$$

Calculation of the Band Structure at the Electrode/Dielectric Interface:

The point where the tangent line to the linear region in the UV diagram intersects the x-axis corresponds to λ_g.

$$E_{\mathrm{g}} = \frac{hc}{\lambda_g}$$

Where: $hc = 1240$; E_g: Bandgap width; h: Planck's constant; c: Speed of light in vacuum.

Based on the testing principle of UPS, it satisfies the following formula:

$$IP_{\mathrm{HOMO}} = hv - (E_{\mathrm{SEE}} - E_{\mathrm{HOMO}})$$

$$\varphi_{\mathrm{h}} = IP_{\mathrm{HOMO}} - \varphi_{\mathrm{m}}$$

$$\varphi_{\mathrm{e}} = E_{\mathrm{g}} - \varphi_{\mathrm{h}}$$

IP_{HOMO}: Ionization potential; hv: Ultraviolet light energy (21.22 eV); φ_h: Hole barrier potential; φ_e: Electron barrier potential. φ_m: Work function of Au (5.2 eV). The secondary electron cutoff (E_{SEE}) and E_{HOMO} values are extracted from the intersection of the baseline and the tangent line of the secondary electron cutoff region/E_{HOMO} region, respectively. Utilizing the IP value, the energy level position of the HOMO is determined, enabling further inference of the LUMO energy level position.

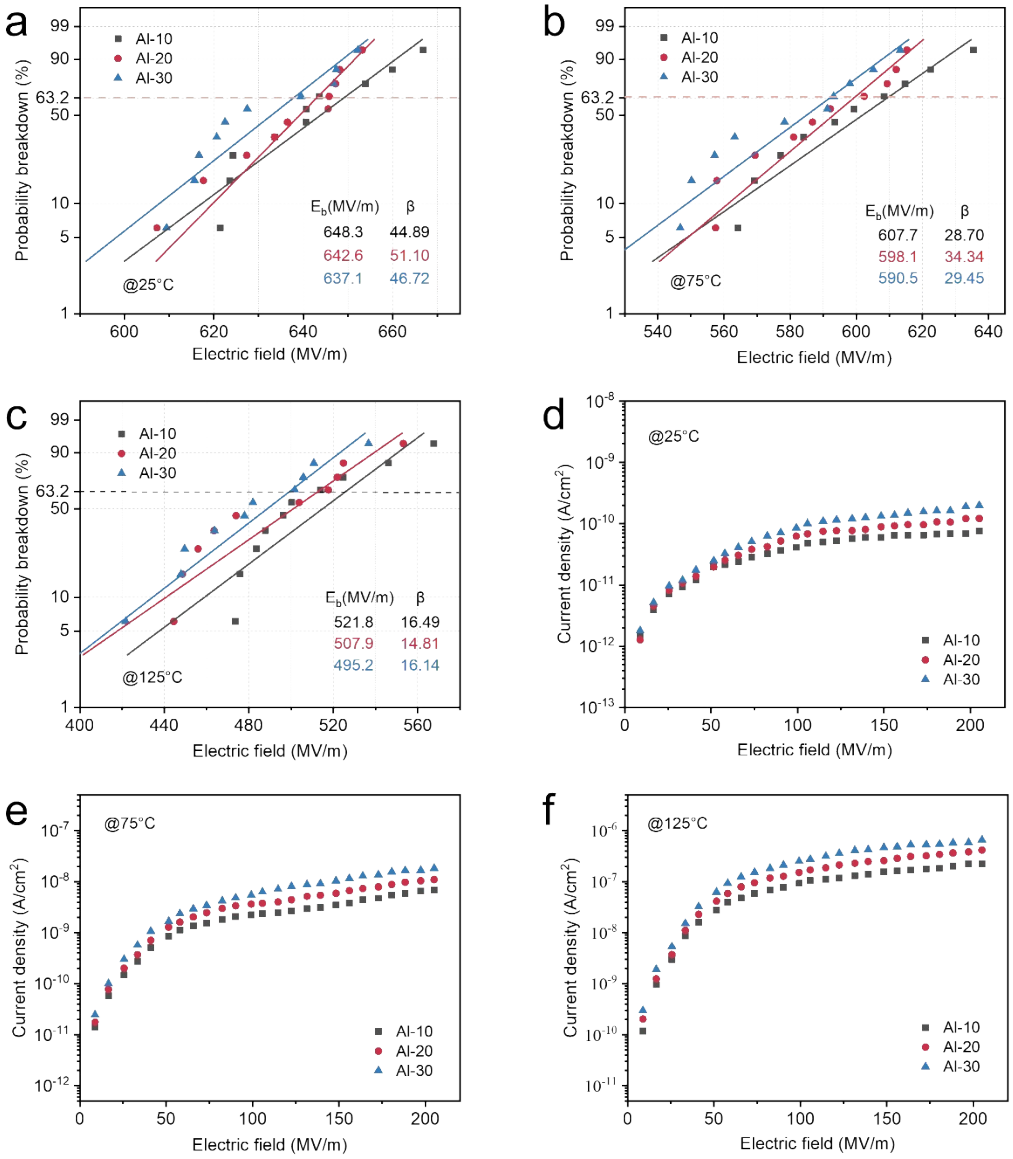

Fig. S1. Breakdown strength of BOPP films with different thicknesses of aluminum metal layer at (a) 25℃, (b) 75℃, and (c) 125℃. Leakage current density of BOPP films with different thicknesses of aluminum metal layer at (d) 25℃, (e) 75℃, and (f) 125℃.

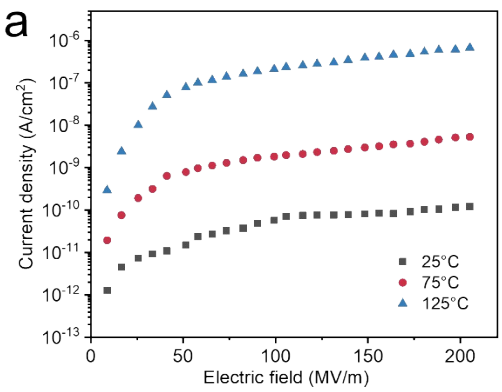

Fig. S2. Leakage current density of BOPP film at different temperatures

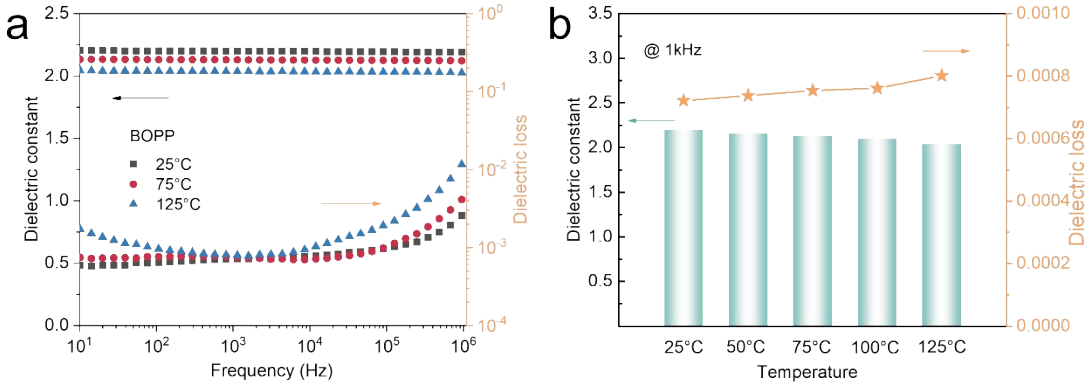

Fig. S3. (a) Frequency dependence of the relative permittivity of BOPP film at different temperatures, (b) Temperature dependence of the relative permittivity of BOPP film at 1 kHz.

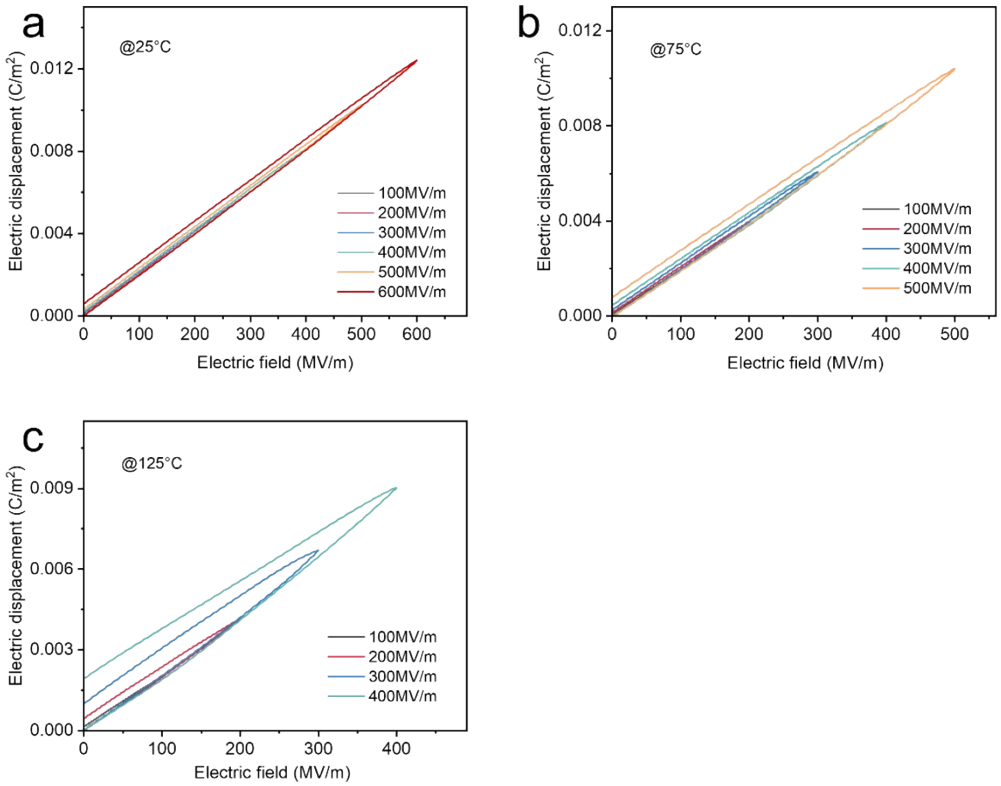

Fig. S4. D-E loops of BOPP film at (a) 25℃, (b) 75℃, and (c) 125℃.

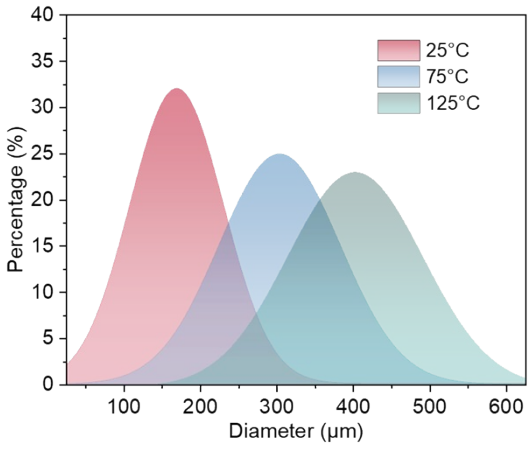

Fig. S5. Breakdown aperture distribution of BOPP film at (a) 25℃, (b) 75℃, and (c) 125℃.

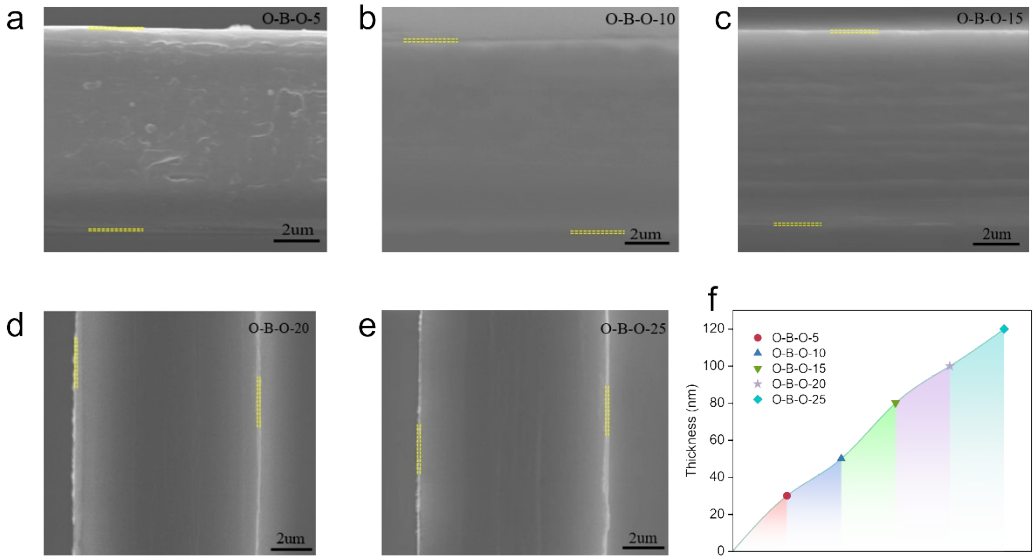

Fig. S6. SEM images of O-B-O composite films with sputtering times of (a) 5 min, (b) 10 min, (c) 15 min, (d) 20 min, and (e) 25 min; (f) Relationship between sputtered thickness and sputtering time.

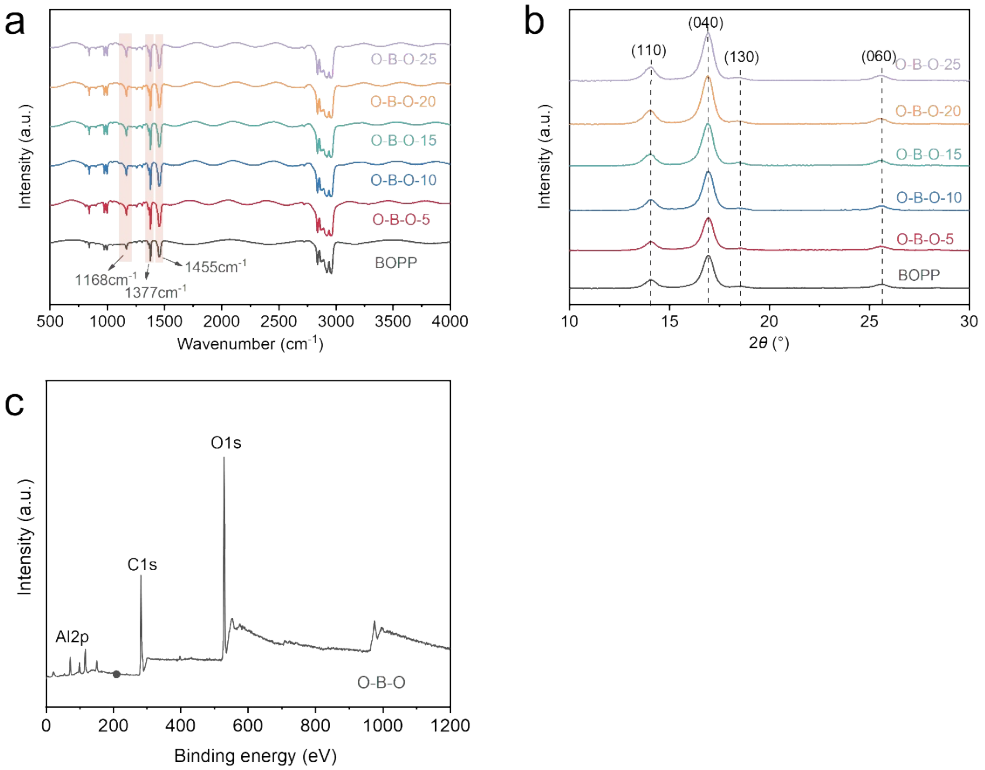

Fig. S7. (a) FTIR spectra and (b) XRD patterns of BOPP, O-B-O-5, O-B-O-10, O-B-O-15, O-B-O-20, and O-B-O-25 films; (c) XPS spectrum of the O-B-O-20 composite film.

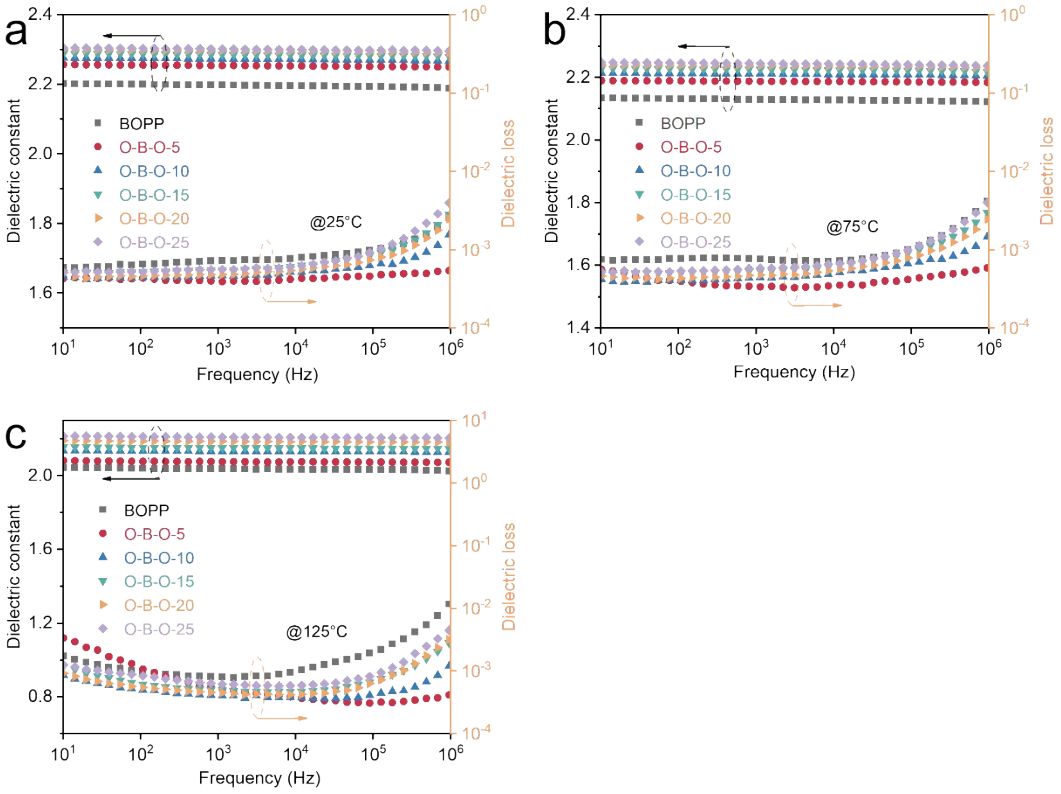

Fig. S8. Frequency dependence of dielectric constant and dielectric loss for BOPP, O-B-O-5, O-B-O-10, O-B-O-15, O-B-O-20, and O-B-O-25 films: (a) at 25℃, (b) at 75℃, (c) at 125℃.

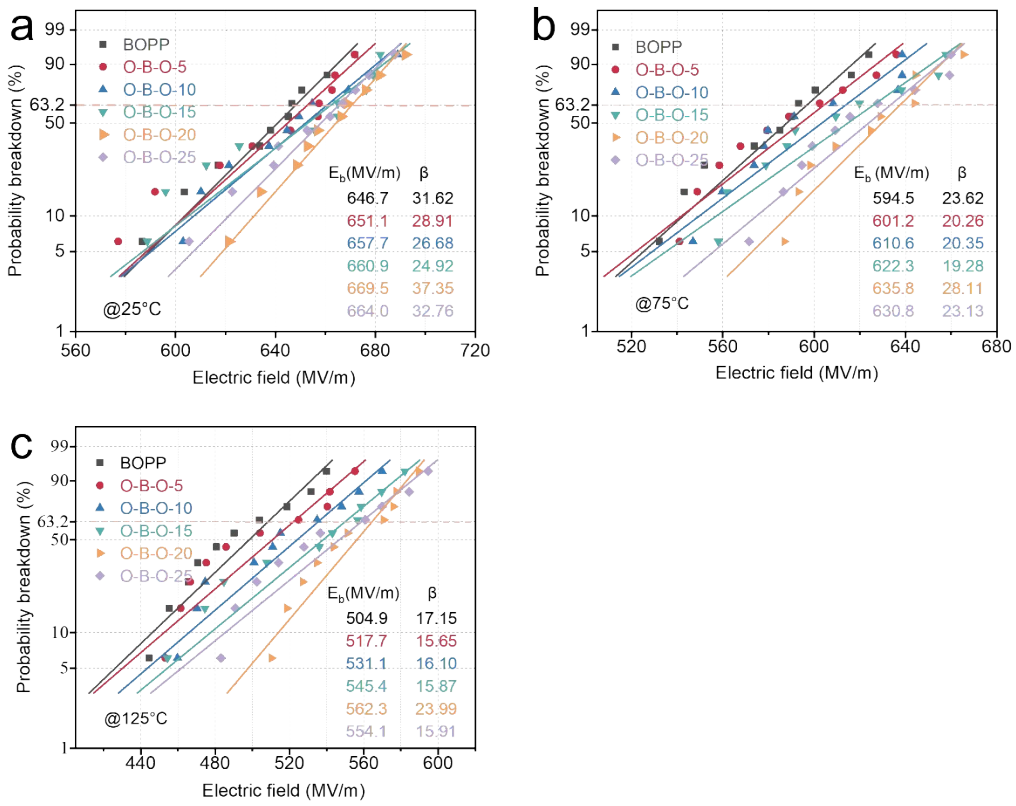

Fig. S9. Breakdown characteristics of BOPP, O-B-O-5, O-B-O-10, O-B-O-15, O-B-O-20, and O-B-O-25 films: (a) at 25℃, (b) at 75℃, (c) at 125℃.

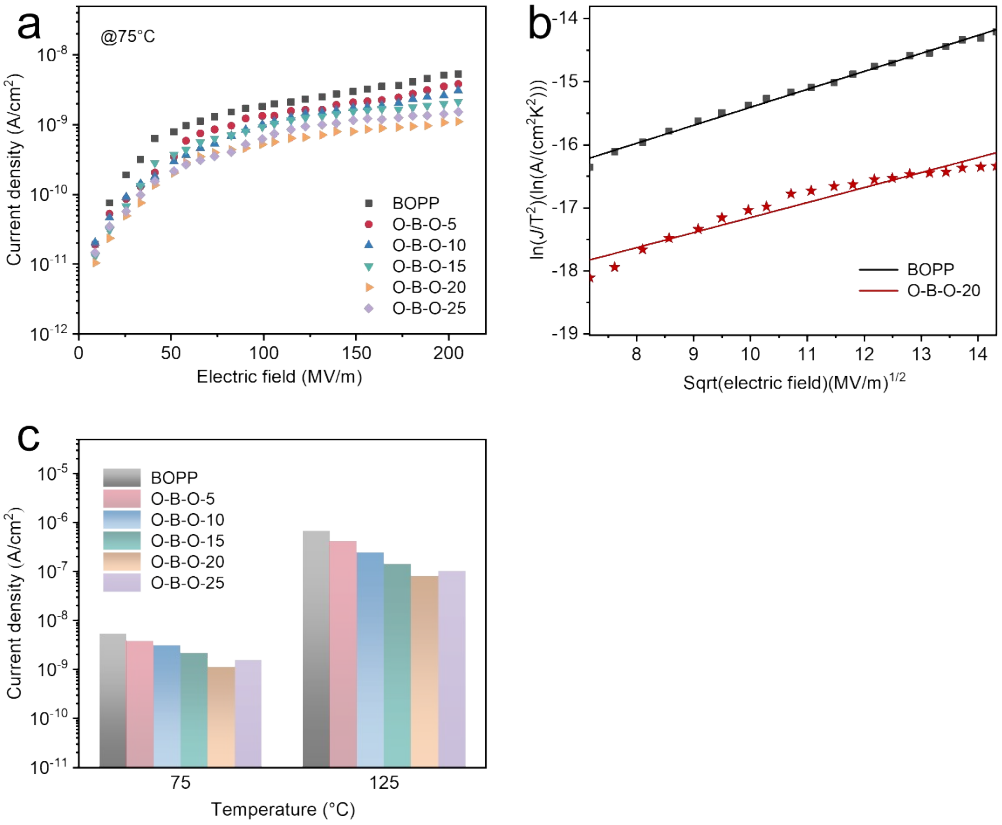

Fig. S10. (a) Breakdown characteristics (75℃) and (c) Leakage current density of BOPP, O-B-O-5, O-B-O-10, O-B-O-15, O-B-O-20, and O-B-O-25 films. (b) Schottky fitting plot of leakage current for BOPP and O-B-O-20 composite films.

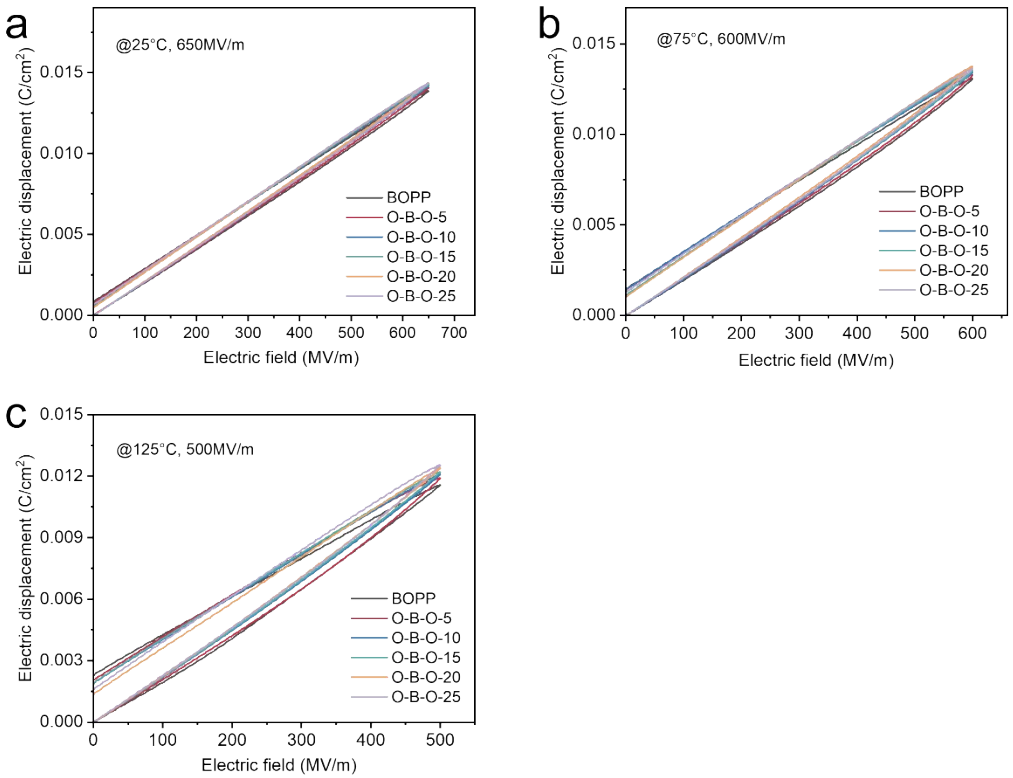

Fig. S11. D-E loop of BOPP, O-B-O-5, O-B-O-10, O-B-O-15, O-B-O-20, and O-B-O-25 films: (a) at 25℃, (b) at 75℃, (c) at 125℃.

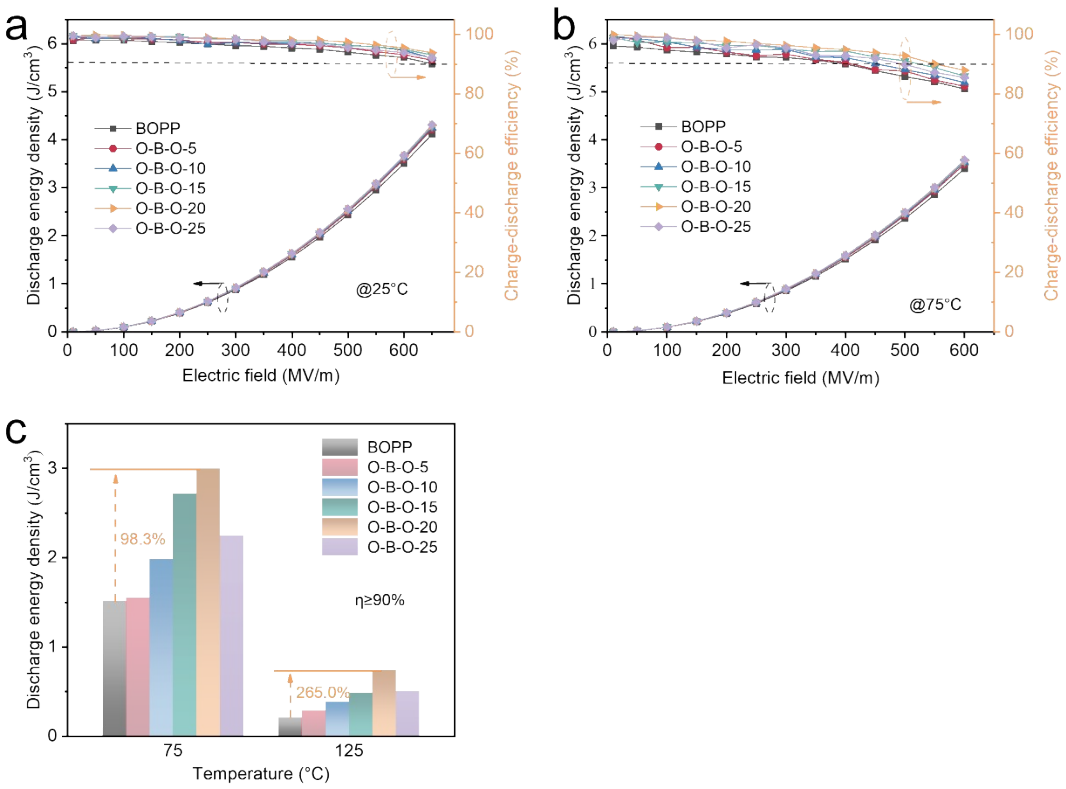

Fig. S12. Energy storage performance of BOPP, O-B-O-5, O-B-O-10, O-B-O-15, O-B-O-20, and O-B-O-25 films: (a) at 25℃, (b) at 75℃, (c) Columnar comparison diagram.

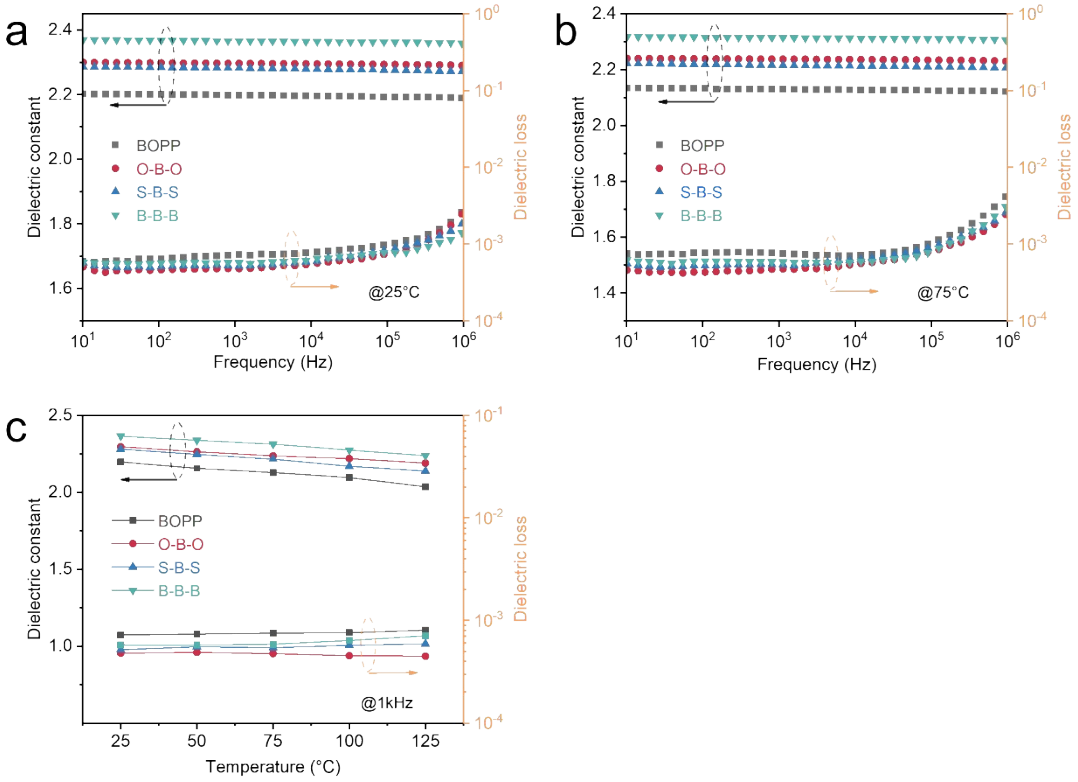

Fig. S13. Frequency dependence of dielectric constant and dielectric loss for BOPP, O-B-O, S-B-S, and B-B-B films (a) at 25℃, (b) at 75℃, and (c) Temperature dependence of dielectric constant and dielectric loss.

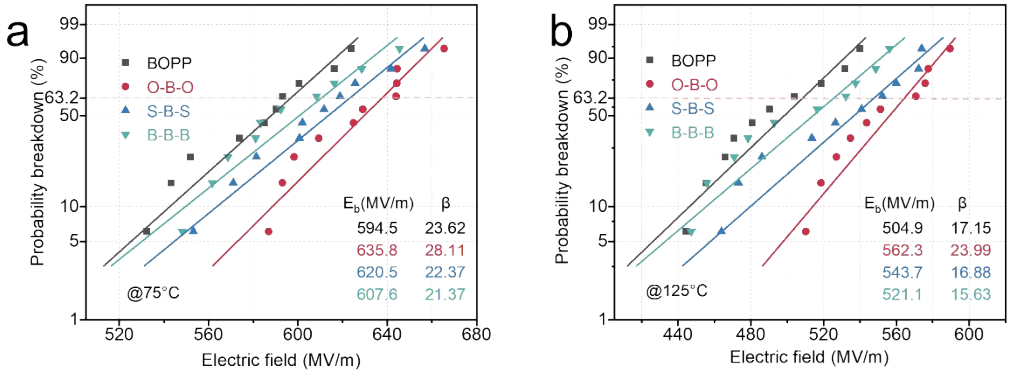

Fig. S14. Breakdown strength of BOPP, O-B-O, S-B-S, and B-B-B films at (a) 75℃ and (b) 125℃.

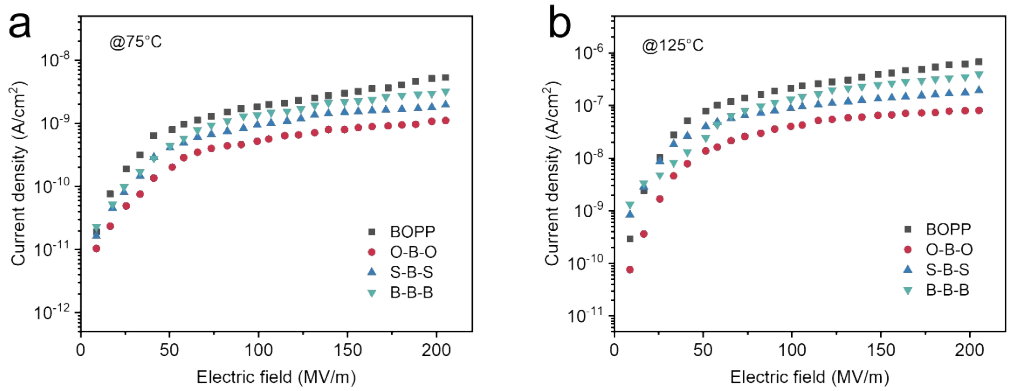

Fig. S15. Leakage current density of BOPP, O-B-O, S-B-S, and B-B-B films at (a) 75℃ and (b) 125℃.

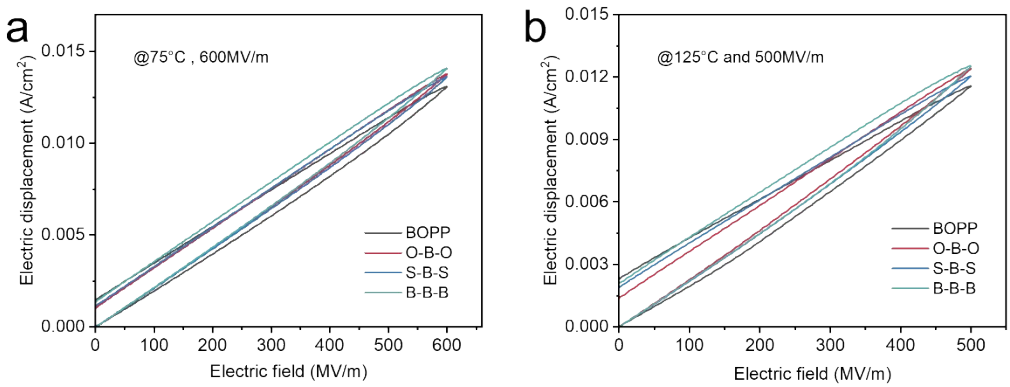

Fig. S16. D-E loop of BOPP, O-B-O, S-B-S, and B-B-B films (a) at 75℃, (b) at 125℃.

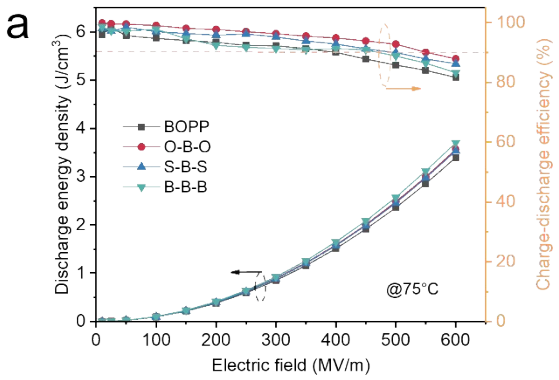

Fig. S17. Energy storage performance of BOPP, O-B-O, S-B-S, and B-B-B films (75℃).